Transparent vs Translucent Multi-Band Optical Networking: Capacity and Energy Analyses

Rasoul Sadeghi ⬵, *Student Member, IEEE*, Bruno Correia ⬵, *Student Member, IEEE*, André Souza ⬵, Nelson Costa ⬵, João Pedro ⬵, *Senior Member, IEEE*, Antonio Napoli ⬵, and Vittorio Curri ⬵, *Senior Member, IEEE*

Abstract—Multi-band optical fiber transmission is generally proposed for capacity upgrades in optical transport networks. To comprehensively assess the potential of multi-band transmission, key metrics such as the potential capacity increase, energy consumption, and the number of required interfaces must be evaluated for different transmission scenarios. We consider progressive spectral exploitation, starting from the C-band only and up to C+L+S+U-band transmission, for both transparent and translucent solutions that exploit optical signal regeneration. By considering accurate state-of-the-art physical layer models, we derive a networking performance metric that enables the comparison of different solutions in terms of capacity allocation and energy consumption. For a translucent network design, different regenerator placement algorithms are compared, with the aim of minimizing energy consumption. The proposed network-wide numerical analysis shows that, for spectral occupations exceeding the C+L-band, translucent solutions can significantly increase network capacity, while leading to a similar energy consumption per transmitted bit as in the transparent design case, but they require the deployment of additional line interfaces. Significantly, these results provide evidence that the transparent exploitation of an additional transmission band produces a capacity increment that is at least comparable to that of a translucent solution based on already-in-use bands. Since this is attained at the expense of fewer line interfaces, it is a key finding suggesting that extending the number of bands supported is a cost-effective approach to scaling the capacity of existing fiber infrastructures.

Index Terms—Optical communication, multi-band optical network, quality of transmission, energy consumption.

Rasoul Sadeghi, Bruno Correia, and Vittorio Curri are with DET, Politecnico di Torino, Corso Duca degli Abruzzi 24, 10129 Torino, TO, Italy (e-mail: rasoul.sadeghi@polito.it; bruno.dearaujo@polito.it; vittorio.curri@polito.it).

André Souza and Nelson Costa are with Infinera Unipessoal, Lda., Rua da Garagem, 1, 2790-078 Carnaxide, Portugal (e-mail: anunes@infinera.com; NCosta@infinera.com).

João Pedro is with Infinera Unipessoal, Lda., Rua da Garagem, 1, 2790-078 Carnaxide, Portugal, and also with the Instituto de Telecomunicações, Instituto Superior Técnico, University of Lisbon, 1049-001 Lisboa, Portugal (e-mail: jpedro@infinera.com).

Antonio Napoli is with Infinera, Munich, Germany (e-mail: ANapoli@infinera.com).

Color versions of one or more figures in this article are available at https://doi.org/10.1109/JLT.2022.3167908.

Digital Object Identifier 10.1109/JLT.2022.3167908

I. INTRODUCTION

THE reliance of our modern society on the Internet has only grown stronger over the years. Forecasts indicate that a steep increase in demand for capacity in telecommunication networks will continue on a worldwide scale as a consequence of, for example, cloud-based applications, high definition streaming, virtual/augmented reality applications, and 5 G deployment [1]. Consequently, it is necessary to implement long-term and cost-effective solutions in optical backbone networks to accommodate the ever-growing traffic requirements while limiting the overall energy consumption of networking equipment [2]. Wavelength division multiplexing (WDM) that exploits only the C-band with a bandwidth of ∼4.8 THz [3] is currently the most commonly deployed and cost-effective solution for transmitting the required data in optical networks, ranging from very long-haul/submarine to metro networks.

Multi-band optical fiber transmission (MBT) is a natural solution to cope with the increasing request of capacity, as it requires fewer changes to existing optical fiber infrastructures. This solution implements transmission over a wider spectral range within the low-loss region of the widely deployed single-mode optical fibers, namely the ITU-T G.652.D type, exceeding a total transmission bandwidth of ≈50 THz [3], [4]. Several works have already shown the potential of MBT, considering several different combinations of spectral bands, from the O- to L-band [5]–[11]. Commercial availability of MBT solutions for C+L-band transmission has also been demonstrated in [12], [13]. One of the key advantages of using MBT to upgrade optical networks is that by relying on the existing optical fiber infrastructure the capital expenditure (CAPEX) is kept low in comparison to other approaches [14], [15]. Adopting a translucent network design can also be used to augment optical network capacity [16]–[21]. In this case, the end-to-end lightpaths (LPs) are divided into several shorter transparent segments via optical-electrical-optical (OEO) signal regeneration at intermediate nodes [22], using standard transceivers (TRXs)/interfaces to perform the signal regeneration. By reducing the length of the LPs to be established, this design strategy aims to enable the use of more spectrally efficient signal formats, hence increasing capacity without resorting to additional spectrum [23]. However, optical signal regenerators are one of the factors that increase cost and energy consumption. Therefore, this is a resource that must be managed efficiently. In both cases, using spectral- and power-efficient interfaces is critical in decreasing

operational expenditures (OPEX) without increasing excessively the CAPEX. Several studies have already addressed the regenerator placement and/or assignment problems. As examples, (i) in [24], the authors focused on the planning and deployment of re-amplification, re-shaping, and re-timing (3R) regenerators accordingly to the network and traffic information; (ii) in [25], two heuristics were proposed for the regenerator assignment. In this case, one of the heuristics targets to deploy the highest order modulation format possible, while the other one tries to reach the maximum transmission distance before performing signal regeneration; (iii) in [26], three metrics were proposed for the regenerator placement focusing on minimizing the network cost, which was evaluated as a function of the total number of regenerators and nodes with 3R capacity; (iv) in [27], the authors focused on minimizing the total number of regenerators when network protection capability was also deployed. (v) in [28] an optimized regenerator assignment strategy based on the QoT of the links was reported. Moreover, a comparison between transparent, translucent, and opaque (which assumes 3R regeneration occurs at every intermediate node) network designs was carried out by Ramamurthy et al. [29], showing that a translucent network design enhances the overall network performance in medium-scale networks where crosstalk and ASE noise are the most limiting transmission effects. However, opaque designs seem more promising for long-haul networks, where nonlinear fiber transmission and chromatic dispersion are the dominant transmission effects. Nevertheless, the comparison between transparent, translucent and the combination of both network designs in MBT scenarios has not been investigated yet. This is a very relevant topic of research because different transmission bands show different Quality of Transmission (QoT) and, therefore, the potential of each network design cannot be simply extrapolated from the conclusion drawn when considering C-band only or C+L-band transmission.

Regarding the energy consumption of interfaces, the effect of complementary metal-oxide-semiconductor (CMOS) node size has been investigated in [30], where it is shown that the CMOS node size is decreasing every two years, with the CMOS power consumption decreasing by about ∼30% in each process step [31]. Recently, the Optical Internetworking Forum (OIF) has defined the 400ZR implementation agreement (IA) [32] where coherent techniques are being introduced in pluggable form factors, aiming to achieve a high capacity and power-efficient interface solution. Particularly, 400ZR defines 400 Gb/s single-wavelength transmission with a symbol rate of 59.84 GBaud using 16-quadrature amplitude modulation (QAM) modulation format, ultimately offering a cost-effective solution for data center interconnect (DCI) applications. The recent OpenZR+ multi-source agreement (MSA) [33], extends the usage of this type of coherent interface to longer transmission systems by slightly increasing its complexity while keeping the target form factor. The support of an improved forward error correction (FEC) code and the ability to use also lower order modulation formats (8QAM, 4QAM) allows supporting a wider variety of applications than 400ZR [34].

In this work, we perform a physical layer aware statistical network assessment [35] by progressively loading the network
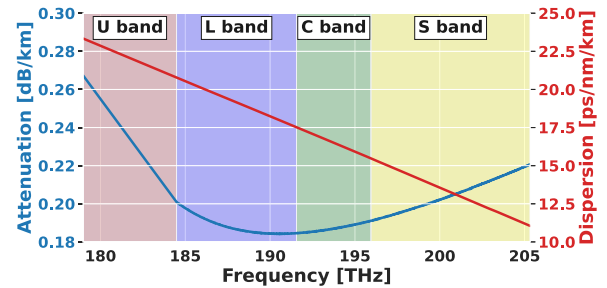

Fig. 1. Attenuation and chromatic dispersion profiles versus frequency for SSMF.

for several MBT transparent and translucent designs to gain insight on key performance metrics, such as capacity, energy consumption, and the number of used interfaces for each scenario. First, we evaluate the impact of loading optical networks with different traffic request sizes, namely with 100 and 400 Gb/s traffic requests. Afterward, three different algorithms are proposed for the optimized 3R regenerator placement in a translucent network design. Two of these algorithms focus on the optimized placement of 3R regenerators in all transmission bands whereas a third one focuses on enhancing the capacity on specific transmission bands only. Finally, the potential of deploying 3R regenerators to decrease the links congestion in MBT scenarios is discussed. A key contribution of this work is to gain insight into the trade-offs from using a specific set of bands (ranging from the U- to the S-band) in combination with a given network design approach. This knowledge can be used, for example, to steer the process of deciding on the most appropriate configuration to scale network capacity according to the specifics of the network scenario and the operator's priorities.

The remainder of this paper is organized as follows. Section II describes the approach to perform the QoT estimation in multi-band scenarios. Section III details the network assessment process, the network physical topology, the traffic pattern, as well as the two network designs used in this work: transparent and translucent. Section IV compares the proposed 3R regenerators assignment algorithms and evaluates the impact of the different network designs in terms of capacity, costs, and energy consumption. Finally, Section V draws the conclusions of the work and provides an outlook of future studies to be carried out.

II. LP QoT EVALUATION IN MBT SCENARIOS

The accurate modeling of signal propagation along an optical fiber, especially in MBT scenarios, requires that the frequency dependence of the fiber parameters (mainly fiber attenuation and chromatic dispersion) is taken into account. As an example, both attenuation and chromatic dispersion dependence on frequency for a standard single-mode fiber (SSMF) are depicted in Fig. 1. In the C- and L-band, the attenuation coefficient of an SSMF is usually <0.2 dB/km whereas it may reach ∼0.22 dB/km in the S-band and further increases up to 0.27 dB/km in the U-band.

Additionally, the stimulated Raman scattering (SRS), a nonlinear effect that causes power transfer from higher to lower frequency signals [36] and that can be mostly neglected in C-band
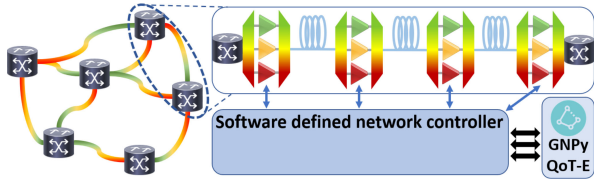
Fig. 2. Optical line system abstraction in a disaggregated approach.

only systems, must be taken into account in MBT systems due to the much broader transmission spectrum. The optical power transfer due to SRS will add on top of the higher fiber loss in the S-band causing this band to have lower QoT than the C- and L-band. Contrarily, despite having a higher fiber loss than the other spectral bands, the U-band benefits from the effect of SRS, receiving optical power from the data channels transmitted in the higher frequency bands.

In this work, the QoT at the end of each fiber span for the i-th channel is computed using the generalized signal-to-noise ratio (GSNR) [37]:

$$\text{GSNR}_i = \frac{P_{S,i}}{P_{\text{ASE},i} + P_{\text{NLI},i}} = \left(\text{OSNR}_i^{-1} + \text{SNR}_{\text{NL},i}^{-1}\right)^{-1}, \quad (1)$$

where $P_{S,i}$ is the span input power, and OSNR_i and $\text{SNR}_{\text{NL},i}$ are the optical signal-to-noise ratio and nonlinear signal-to-noise ratio, respectively. In this case, we are assuming that the LPs optical performance degradation results from two main contributors: the amplified spontaneous emission (ASE) noise and the nonlinear interference (NLI) noise introduced by optical amplifiers and fiber propagation, respectively. Both effects can be approximated as Gaussian disturbances for most of the relevant transmission scenarios. The ASE noise power ($P_{\text{ASE},i}$) is given by:

$$P_{\text{ASE},i} = h f_i \text{NF}(f_i) G(f_i) B_{\text{ref}}, \quad (2)$$

where h is the Planck's constant, B_{ref} is the reference bandwidth, and $G(f_i)$ and $\text{NF}(f_i)$ are the gain and noise figures of the optical amplifiers measured in the frequency of the i-th channel, f_i, respectively. The NLI power ($P_{\text{NLI},i}$) contribution is computed using the Generalized Gaussian Noise (GGN) model [38], which takes into account the effects of spectral and spatial variations of fiber loss and the SRS-induced inter-channel power crosstalk.

Finally, following a disaggregated abstraction of the physical layer [39], [40], the total QoT of an LP l is computed by:

$$\text{GSNR}_{i,l} = \frac{1}{\sum_{s \in l}(\text{GSNR}_{i,s})^{-1}}, \quad (3)$$

which depends on the GSNR of each fiber span s traversed by the LP under test. The open-source GNPy library [41] implements the described QoT estimation methodology. Given the extensive use of this library, it is now a robust implementation of the methodology and, therefore, it is used in this work.

In MBT scenarios, and as illustrated in Fig. 2, several optical amplifiers are needed at each amplification site (at least one for each transmission band). This approach is implemented to cope with the limited amplification bandwidth and maximum output power of existing optical amplifiers. For the same reason, we
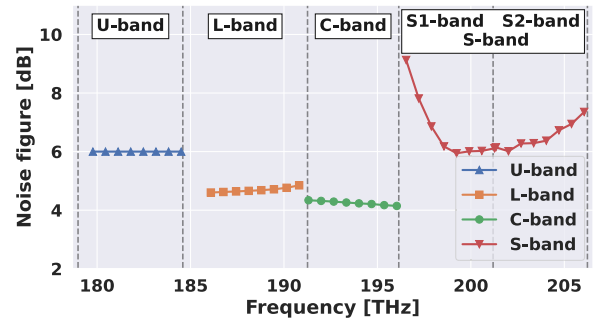

Fig. 3. Noise figure for the U-, L-, C-, and S-band optical amplifiers.
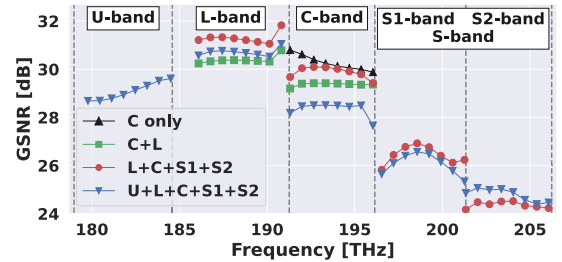


Fig. 4. GSNR profile in a single span of 75 km.

assume also the split of the S-band in two identical sub-bands: here named S1- and S2-band, to lessen the requirements on the S-band amplifier. By following this approach, two optical amplifiers are used in the S-band, one for each sub-band, whose required amplification bandwidth and output power should be similar to the ones of the C- and L-band optical amplifiers. Erbium-doped fiber amplifiers (EDFAs) provide enough amplification in C- and L-band. However, their performance degrades significantly when used in other transmission bands and, therefore, different doping materials are required in these cases [3]. Thus, we consider lumped EDFA amplification for the C- and L-band, and the use of a bench top thulium-doped fiber amplifier (TDFA) for the S-band, characterized as reported in [42]. Average noise figures (NF)s of 4.3 dB, 4.7 dB, and 6.5 dB are assumed for the C-, L-, and S-band optical amplifiers, respectively. The TDFA shows a higher NF mainly because of the not yet fully mature technology. Similarly, optical amplifiers for the U-band are still in an early stage of development and, therefore, reliable characterization data is still hard to obtain. Consequently, we assume that the U-band optical amplifiers can be approximated by a flat NF of 6.0 dB. The resulting noise figure as a function of frequency is illustrated in Fig. 3 As also highlighted in Fig. 2, the transmission bands in a MBT system need to be separated/combined before/after optical amplification. Consequently, MBT leads to increased insertion losses, when compared to single-band transmission, resulting from the multiplexing and demultiplexing of the different bands (which are assumed to be of 1 dB for each operation [43], [44]). Additionally, a guard band of 0.5 THz is also set between each band. Fig. 4 depicts the GSNR profile after transmission of 64 channels with symbol rate of 64 GBaud in the 75 GHz WDM grid along a single 75 km ITU-T G.652D optical fiber span (whose

TABLE I
AVERAGE GSNR [DB] FOR DIFFERENT MTB SCENARIOS

band	U	L	C	S1	S2
GSNR	–	–	30.25	–	–
	–	30.37	29.38	–	–
	–	31.28	29.94	26.48	24.38
	29.08	30.69	28.42	26.13	24.79

attenuation and chromatic dispersion are modelled as shown in Fig. 1 and with a nonlinear fiber coefficient of 1.27 W^{-1}/km), for all four MBT scenarios considered in this work: (i) C-band only; (ii) C+L-band; (iii) L+C+S1+S2-band; and (iv) U+L+C+S1+S2-band. Please note that MBT should be seen as a future-looking solution to tackle traffic growth; consequently, the use of at least current state-of-the-art TRXs should also be assumed in combination with MBT. Thus, this assumption corresponds to using 64 Gbaud TRXs and the corresponding channel spacing of, at least, 75 GHz.

The launch power is optimized for each MBT scenario separately, targeting the QoT maximization in all bands. The local-optimization, global-optimization (LOGO) [45] approach is used to compute the starting point of the launch power per channel in each band. In this case, a per-channel launch power of 0.6, 1, and 2.9 dBm is estimated for the C-, L- and U-bands, respectively, whereas 1.4 and 1.7 dBm are estimated for S1 and S2 within the S-band, respectively. Starting from these initial estimates, and as described in [46], we then run a multi-evolutionary algorithm to find the optimum average launch power and tilt that maximizes the average GSNR in each band while still maintaining an acceptable GSNR flatness. Comparing the reference case (C-band only transmission) with C+L-band transmission, Fig. 4 shows that the latter presented a GSNR decrease of about 1 dB in the C-band. This degradation of optical performance results from the SRS effect, which transfers power from the C-band into the L-band. Consequently, higher ASE noise is added to the C-band by optical amplifiers when recovering the signal power. Regarding the L-band, the best GSNR is attained for the C+L+S1+S2-band transmission scenario, as a consequence of receiving power from all other bands. In this case, smaller ASE noise is added by optical amplifiers when compensating for the link loss. Similarly, Fig. 4 show also that in the C+L+S1+S2+U-band transmission scenario, the performance of C-band can be significantly impacted, presenting a GSNR penalty of about 2 dB, mainly due to the power transfer from the C-band to the U-band. The average GSNR value in each band for each considered MBT scenario is presented in Table I. The average is computed among all channels within the band, also for a single span of 75 km. As expected, the best QoT is achieved in the C- and L-band. Moreover, the S-band is the one showing the worse QoT, mainly as a consequence of power depletion caused by the SRS effect. Indeed, the GSNR attains almost 31 dB in the best performing LP in the C-band only transmission scenario, whereas it decreases to about only 25 dB in the best performing LP in the S2-band. The dependence of the QoT, in each band, on the actual MBT scenario is also clear from this set of results, where it is shown that the optical
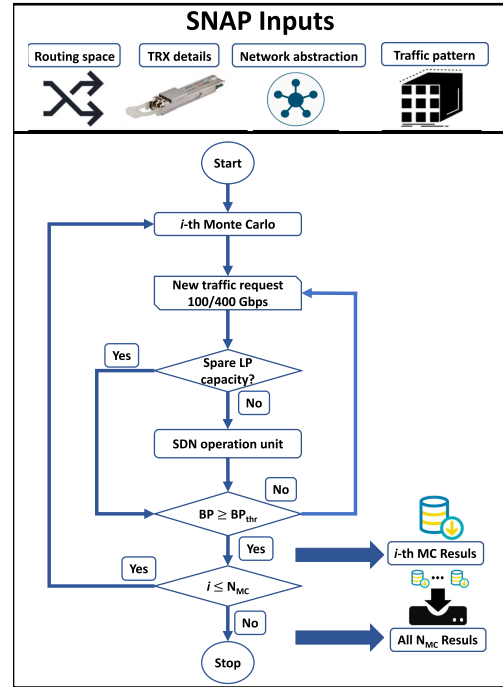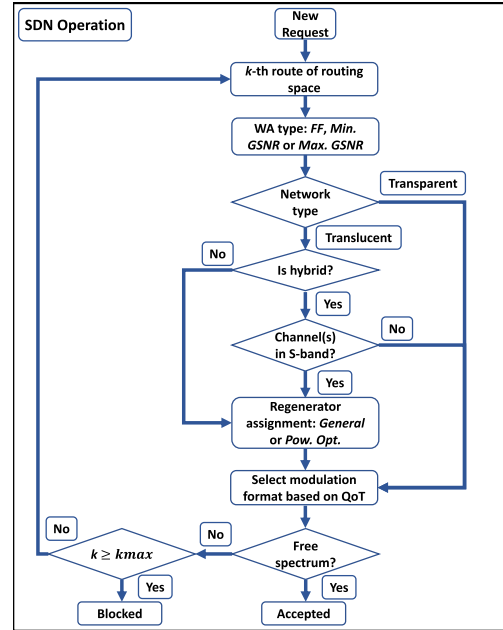
Fig. 5. Flowchart of the a) SNAP and b) SDN operation unit.

performance of each band may increase or decrease depending on the activation status of the neighbor bands. Interestingly, only a small variation of the QoT within each band is usually obtained independently of the considered MBT scenario, which might potentially reduce the complexity of routing and spectrum assignment algorithms. After the QoT of the LP is computed, the Software-Defined Networks (SDN) controller (depicted in Fig. 5(b)) can determine the most spectrally efficient modulation format that can be used based on the obtained GSNR. The

Mod. Form.	Data rate [Gb/s]	P [W]	RGSNR [dB]
16QAM	400	20	21
8QAM	300	18	18
QPSK	200	16	14

interface type used in this work is based on the OpenZR+ MSA [33], but considering better performing interfaces [47]. The main properties assumed per modulation format are shown in Table II. Three modulation formats are supported: 16QAM, 8QAM, and quadrature phase-shift keying (QPSK). The interface performance for each modulation format is set by the required (minimum) GSNR (RGSNR) for error-free transmission operation. This RGSNR is obtained from the pre-FEC bit-error rate (BER) versus the optical signal to noise ratio (OSNR) curve by measuring it at the BER threshold [40]. The analysis of Table II shows that the use of a more efficient modulation format leads to an increase in power consumption. However, the power consumption normalized to the offered capacity actually decreases. This reinforces the relevance of exploiting the most spectrally efficient modulation format that is feasible in each LP.

III. METHODOLOGY AND METRICS

The methodology employed to estimate the overall network performance and the metrics used to evaluate the different network designs are described in this section. The network evaluation is performed using the statistical network assessment process (SNAP) framework [35], which uses the GSNR (Section II) as the QoT metric. The SNAP framework has been customized to cover both transparent and translucent network design scenarios.

A. SNAP Flowchart Description

Figure 5 presents the SNAP flowchart that has been used to statistically test the network, which is a Monte Carlo (MC) based procedure comprising two main parts. The first part, shown in Fig. 5(a), is the high-level workflow view containing the input variables, such as the traffic pattern, network abstraction, interface parameters (TRX parameters), and routing space. A progressive traffic loading [35] is used. In this case, different traffic patterns can be selected by changing the joint probability density function (JPDF) of the nodes. For example, uniform (considered in this work) or population-based JPDF can be chosen [36].

As shown in Fig. 5(a), the network abstraction is performed using GNPy, which provides a weighted graph corresponding to the QoT per channel. The k-shortest path algorithm is then used to find the first five shortest paths among all source and destination node pairs ($k_{max} = 5$ in this work). The MC simulation starts after defining all input variables. This simulation approach relies on repeated random sampling to obtain the numerical results. In order to compute networking metrics with high confidence, a total of 1000 MC iterations is considered.

For network analysis, the SNAP can load the network with 100 and 400 Gb/s traffic requests. As a consequence, the capacity of some LPs may not be immediately fully exploited when setting up a new traffic demand, i.e., when the available QoT allows creating a LP with a capacity higher than the one requested by the new demand. Hence, as shown in Fig. 5(a), SNAP verifies if there is any existing LP with the same source and destination nodes with enough spare capacity to support the new request before creating a new LP. If spare capacity is found, the new traffic demand will use the already deployed LP, avoiding the increase in cost and power consumption associated to creating new LPs. Otherwise, the SDN operation unit (Fig. 5(b)) will try to establish a new LP based on the network design strategy and the routing, and wavelength assignment policies. In case a new LP needs to be established, the SDN operation unit starts to do the wavelength assignment from the first shortest path, according to the wavelength assignment policy chosen. The policies tested in our framework are described in Section III-C. Then, the SDN unit selects the best (highest capacity) available modulation format based on the QoT. Afterwards, it assesses if there are resources available to serve the traffic request with the selected modulation format.

Please note that the SDN unit is also responsible for selecting the nodes where LP regeneration takes place in a translucent network design. Different algorithms can be used in this case. The ones considered in this work are described in Section III-D. Particularly, a hybrid network design, where regeneration is only considered for the channels within a spectral band with low QoT (S-band in our case), is also considered in this work. The network blocking probability (BP) is evaluated after routing each traffic demand. If it exceeds a given threshold ($BP_{thr} = 20\%$ in our case), the current MC iteration is concluded. In that case, the network simulation data is stored and a new MC iteration begins, continuing until the total number of iterations is performed.

B. Topology and Traffic Requests (100/400 Gb/s)

The potential of MBT for capacity upgrade is assessed in the US-NET reference topology. As illustrated in Fig. 6, this network topology consists of 24 optical nodes and 43 edges, with an average nodal degree of 3.6 and an average link length of 308 km [42].

We start by evaluating the impact of loading the network with 100 or 400 Gb/s traffic requests only. In case the QoT of the selected LP required to directly carry a 400 Gb/s traffic request is insufficient, this traffic request is divided into two or more lower capacity requests. In the extreme case, four 100 Gb/s LPs may be set to carry a single 400 Gb/s traffic request. Fig. 7(a) shows the total allocated traffic versus BP using a transparent network design for both request types. In the C-band only transmission scenario, more traffic is supported for a BP of 1% when loading the network with 400 Gb/s connection requests than with 100 Gb/s ones. The higher network capacity in the case of serving 400 Gb/s connection requests is a consequence of having a limited number of wavelengths/channels only. Indeed, in case of C-band only transmission and when serving 100 Gb/s connections, we may reach a quick network saturation without
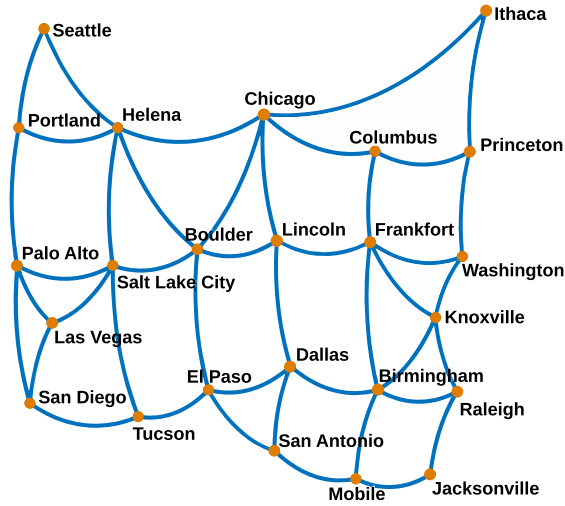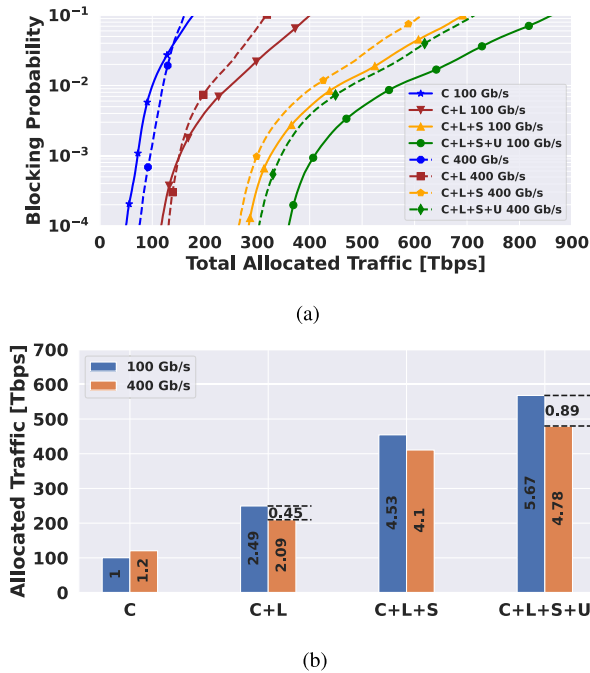
Fig. 6. US-NET topology.

(a)

(b)

Fig. 7. (a) Total allocated traffic in the US-NET topology with serving 100 Gb/s and 400 Gb/s traffic requests for different BPs and (b) the MF of allocated traffic at the BP of 1%.

fully using the existing LPs total capacity. However, by exploiting MBT, the advantage of serving 100 Gb/s traffic requests becomes clear due to the more efficient use of the available QoT and management of the existing LPs. Fig. 7(a) clearly illustrates this behavior. In the C-band only transmission scenario, having 100 Gb/s connection requests leads to smaller allocated traffic for the same blocking probability when compared to 400 Gb/s connection requests for the most relevant BPs. Only for heavily loaded networks, leading to (BP $> 10^{-2}$), having 100 Gb/s connection requests may be beneficial. However, for the C+L-band transmission scenario, having 100 Gb/s connection requests may already be beneficial for BP as low as 10^{-3}. When using even

more transmission bands, having 100 Gb/s connection requests always leads to higher allocated traffic than 400 Gb/s connection requests for all relevant BPs.

Fig. 7(b) depicts the allocated traffic multiplicative factor (MF) for all scenarios at the BP of 1%. The network capacity using C-band only transmission with serving 100 Gb/s traffic requests is used as a reference (solid blue curve in Fig. 7(a)). According to Fig. 7(b), the total allocated network traffic in the case of C-band with serving 400 Gb/s traffic requests is about 1.2 times higher than the one supporting 100 Gb/s traffic requests. However, by doubling the number of available channels (exploiting the L-band), the allocated traffic increases by about 2.49 and 2.09 times in the cases of serving 100 Gb/s and 400 Gbs traffic requests, respectively. This result highlights that the total allocated traffic serving 400 Gb/s traffic requests in a network leads to a drop of 18% in the MF. Moreover, in the C+L+S+U-band MBT scenario (green curves in Fig. 7(a)), this difference is 16% (5.67 and 4.78 with serving 100 Gb/s and 400 Gb/s traffic requests, respectively). This preliminary analysis shows that optical networks operating with 100 Gb/s connection requests may benefit more from the MBT upgrade in terms of total allocated traffic. In the remainder of this work, we focus our analysis solely on supporting 100 Gb/s traffic requests.

C. Transparent Network Design

In view of Fig. 5(b), SNAP supports three different wavelength assignment (WA) policies, namely first-fit (FF), minimum GSNR margin (min. GSNR), and maximum GSNR margin (max. GSNR). The FF spectrum allocation policy used in this work prioritizes the channels with lower frequencies over the higher-frequency channels. The main goal of this well-known WA policy is to pack as many as possible LPs on one part of the spectrum (or spectrum band), keeping the other part free to establish future LPs when the network is more loaded. In the remaining WA policies (min. GSNR and max. GSNR) SNAP has to evaluate the difference (margin) between the GSNR of every channel and the RGSNR of the possible modulation formats. Firstly, the highest-order modulation format feasible over the LP is determined. This consists of the modulation format with the highest capacity for which at least one available channel has a GSNR equal to or higher than the RGSNR. All available channels that also support this modulation format are identified and then ordered based on the GSNR margin, from higher to lower for the max. GSNR method and from lower to higher for the min. GSNR policy. The min. and max. GSNR margin WA policies seemed promising to increase network capacity since they explore better the existing QoT. However, in all investigated scenarios, we found that FF performed better than or similar to these WA policies. This is because, in the long-term and as the network becomes more loaded, FF is more effective in keeping the diminishing number of free channels available in the same spectrum slots over consecutive links (i.e., verifying the spectrum continuity constraint). Consequently, the results shown in the remaining of the paper always assume FF as the WA method.

Algorithm 1: General Translucent Algorithm.

Input: Channel (ch), source / destination route path ($path_{tot}$), list of RGSNR for all modulation formats (RGSNR$_{list}$)

Output: LP regeneration paths ($path_{reg}$)

1:   RGSNR$_{aux} \leftarrow 0$
2:   $path_{temp}, path_{pre}, path_{reg} \leftarrow \emptyset$
3:   **while**RGSNR$_{list} \neq \emptyset$ AND LP not allocated **do**
4:      RGSNR$_{aux} \leftarrow$ Highest RGSNR of RGSNR$_{list}$
5:      RGSNR$_{list} \leftarrow$ RGSNR$_{list} \setminus$ RGSNR$_{aux}$
6:      **for all** links (l) in $path_{tot}$**do**
7:         $path_{temp} \leftarrow path_{temp} \cup l$
8:         **if** GSNR($path_{temp}, ch$) $\geq$ RGSNR$_{aux}$ **then**
9:            $path_{pre} \leftarrow path_{temp}$
10:         **else**
11:            **if** GSNR($path_{pre}, ch$) $\geq$ RGSNR$_{aux}$ **then**
12:               $path_{reg} \leftarrow path_{reg} + path_{pre}$ $\triangleright$ New added transparent segment
13:               $path_{temp}, path_{pre} \leftarrow l$
14:            **else**
15:               **break** $\triangleright$Not enough QoT for single link
16:         **if** l is the last link **then**
17:            $path_{reg} \leftarrow path_{reg} + path_{temp}$ $\triangleright$ New added transparent segment

---

Algorithm 2: Power-Optimized Translucent Algorithm.

Input: Channel (ch), source / destination route path ($path_{tot}$)

Output: LP regeneration paths ($path_{reg}$)

1:   $P_{best} \leftarrow \infty$ $\triangleright$Powers
2:   $C \leftarrow$ Combinations ($path_{tot}$) $\triangleright$ All regeneration possibilities of a path
3:   $R_b, path_{reg} \leftarrow \emptyset$
4:   **for all** c in C **do**
5:      $P_{temp} \leftarrow 0$
6:      **for all** s in c **do** $\triangleright$Transparent segments (s) which composed the LP
7:         $R_b \leftarrow R_b \cup$Capacity (s, ch) $\triangleright$ Bitrate for the specific channel
8:         $P_{temp} \leftarrow P_{temp} +$Power ($s, ch$) $\triangleright$ Power for the specific channel
9:      **if** $P_{temp} \leq P_{best}$ AND All r_b in R_b are equal **then**
10:         $P_{best} \leftarrow P_{temp}$
11:         $path_{reg} \leftarrow c$

D. Translucent Network Design

A translucent network design consists in enabling the regeneration of the optical signal in intermediate nodes. In this case, we assume the use of 3R regenerators, where OEO operation is performed. Although possible, the potential benefit enabled by 3R regenerators of also performing wavelength conversion is not explored. Three different 3R regenerator placement algorithms are considered. Two of them can be used to assign 3R regenerators in any band whereas the last one focuses on placing

3R regenerators in the S-band only, since this band presents the lowest QoT in comparison to the other bands (refer to Fig. 4). The efficiency of the three different algorithms is compared in terms of total allocated traffic, consumed energy per Terabit, interface count as a cost, and allocated LPs. Each 3R regenerator receives and transmits signals at an intermediate node, and therefore, each device counts as two interfaces.

1) General: Algorithm 1 describes the general method for 3R regenerator placement based on the QoT of the LP. This method creates an LP using the most efficient modulation format possible, while simultaneously implementing the highest possible spectral efficiency (SE) that avoids using unnecessary interfaces. The algorithm inputs are: channel (ch), source and destination route path ($path_{tot}$) and a list of RGSNR for all modulation formats supported by the TRXs (RGSNR$_{list}$); the output of this algorithm is an LP with the indication of the regeneration nodes ($path_{reg}$), if any. After the initialization (lines 1 and 2), the algorithm starts by trying the most efficient modulation format and saves it in an auxiliary list, $RGSNR_{aux}$ (lines 3-5). Then, it iterates over the path links (l) and saves the current link in the temporary path list ($path_{temp}$ (lines 6 and 7). Afterwards, it checks the range of the modulation format and determines which intermediate nodes are reachable. When an unreachable node is found (line 10), a regenerator is assigned to the last reachable node defined in $path_{pre}$ (lines 12 and 13). If $path_{temp}$ containing the last link l has enough QoT to reach the last node, it is added to $path_{reg}$ (lines 16 and 17) and the algorithm is finished. However, if there are any links that are unable to support this modulation format, the loop terminates and a new attempt is carried out using a modulation format that requires a lower RGSNR (e.g., 8QAM and QPSK) (line 15). Please note that the worst-case complexity of this algorithm is $O(G \cdot l)$, where l and G are the number of links in the LP and the number of available modulation format, respectively.

2) Power-Optimized (Pow. Opt.): Algorithm 2 describes the Pow. Opt. method/policy for 3R regenerator placement at intermediate nodes. Similarly to the General algorithm, it is based on the QoT of the LPs. However, it also factors in power consumption. Firstly, this algorithm finds all possible regeneration combinations for the LP (C in line 2). Then, it considers each combination (c) and, for all transparent segments (s) of the LP, it computes the bit rate and estimates the power consumption (lines 4-8) and saves it in the R_b and P_{temp} lists. At the end of the iteration, the combination leading to the lowest power consumption and equal bit rate for all transparent segments r_b is selected (line 9-11). Although this algorithm causes a small decrease in the total allocated traffic in comparison to the General algorithm, it has the ability to reduce the energy consumption per Terabit by selectively decreasing the number of 3R regenerators installed. The worst-time complexity of this algorithm is $O(n \cdot 2^n)$, where n is the number of nodes in the LP.

3) Hybrid Multi-Band: From the GSNR profiles presented for a single span in Fig. 4, along with their average values for different bands as given in Table I, we observe that the S-band QoT is worse than the C-, L-, and even U-bands. For this reason, employing signal regeneration devices on wavelengths within
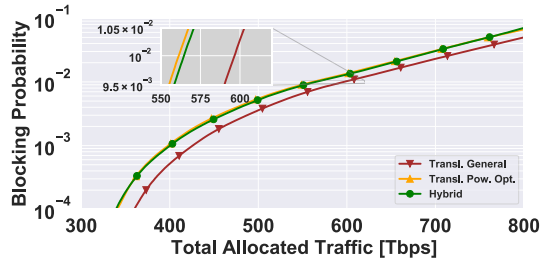
Fig. 8. Network performance in the translucent MBT scenario (C+L+S-band) using the Hybrid, General and Pow. Opt. algorithms for different BPs. The C- and L-bands contain the same number of wavelengths, $N_{ch} = 64$. The S-band contains 128 channels, $N_{ch} = 128$.
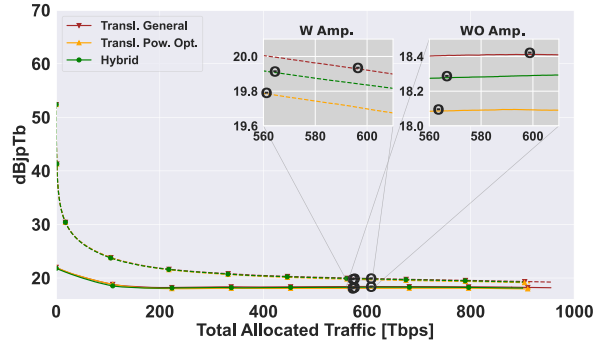

Fig. 9. Energy consumption in a translucent C+L+S MBT design using the Hybrid, General and Pow. Opt. algorithms for different allocated traffics with (dashed curves) and without (solid curves) considering the amplifiers' power consumption. The BP value of 1% is indicated in the figure by θ.

this lower QoT spectral band can lead to capacity increases comparable to the better-performing C- and L-bands. In the following, this approach is designated as Hybrid multi-band [47]. The Hybrid approach can provide a more evenly distributed LP capacity within the network, as it becomes possible to transmit similar data rates across the different bands. This is an important benefit from an operational perspective, by allowing higher layers to assume a single channel capacity figure for a given pair of end nodes, i.e., independently from the band the optical channel will be allocated to. Moreover, it can also lead to reductions in energy consumption and costs when compared to the General algorithm approach. Note that the Hybrid approach enforces the use of the General Algorithm for the regenerator placement in the S-band (see Fig. 5(b)).

IV. RESULTS AND DISCUSSION

This section presents the results for the network topology depicted in Fig. 6 and is divided into two subsections, namely IV-A and IV-B. In the former one, the impact on the network performance of using the General, Pow. Opt. and Hybrid 3R regenerator assignment algorithms for the translucent network design is assessed. In the latter, a comprehensive network analysis is done considering a wide set of MBT scenarios in terms of total allocated traffic, energy consumption, number of used interfaces and links congestion.

A. 3R Assignment Algorithm Comparison

The evaluation of network performance for the different translucent network designs considered in this work (General, Pow. Opt., and Hybrid) is presented in this subsection. Fig. 8 shows the progressive total allocated traffic versus BP for a translucent C+L+S-band network, using the General, Pow. Opt., and Hybrid algorithms, with 256 channels in total (C- and L-band containing 64 channels each and the S-band containing 128 channels). The General algorithm provides the highest delivered capacity for the entire range of BP values shown, as this approach prioritizes the most efficient modulation formats and, consequently, optimizes the capacity of each LP. Conversely, the Pow. Opt. algorithm provides smaller capacity for all BP values, as it focuses on power consumption minimization by reducing/limiting the number of assigned 3R regenerators. In the hybrid case, where signal regeneration occurs in the S-band

only, the network performance in terms of total allocated traffic is similar to the translucent network with Pow. Opt. algorithm. According to Fig. 8, the total allocated traffic in a translucent network design with the Pow. Opt., Hybrid and General algorithms is 561, 564 and 596 Tbps at a BP $= 1\%$, respectively.

We now analyze the total energy consumption for each translucent algorithm using the interfaces power consumption provided in Table II,. Besides the interfaces, the optical amplifiers power consumption is also taken into account. The consumed power of a single amplifier is assumed to be 20 Watts for the C-band [49] and 30 Watts for the L- [50], S- [51], and U-bands. Given the lack of commercially available amplifiers for the U-band, we assumed the highest value among the used options. Using equal spans of 75 km, a total of 173 amplifiers, for each band, are deployed in the US-NET topology. Both energy analyses, with (W Amp.) and without (WO Amp.) considering the amplifiers power consumption, are shown in Fig. 9 (dashed and solid line curves, respectively). The energy consumption is shown in dB Joule per Terabit (dBjpTb) versus the progressively allocated traffic, i.e., the average consumed energy per Terabit is evaluated by dividing the total consumed power by the amount of allocated traffic. The θ symbol in Fig. 9 highlights the result for BP $= 1\%$. For this BP value, considering the amplifiers power consumption increase the energy consumption by about 1.5 dB. As expected, the consumed energy in a translucent network design with Pow. Opt. algorithm presented the lower value when compared with the other algorithms. For instance, when neglecting the amplifiers' power consumption and at a BP of 1% (shown in the right zoom plot), using the Pow. Opt. algorithm leads to a energy consumption of about 18.1 dBjpTb, while this value exceeds 18.3 dBjpTb when using the other algorithms. When taking into account the amplifiers' power consumption, the difference in energy consumption when using the different algorithms decreases. For instance, at a BP $= 1\%$, while using the General algorithm leads to an energy consumption of about 19.9 dBjpTb, using the Pow. Opt. and Hybrid algorithms leads to an energy consumption of about 19.8 and 19.9 dBjpTb, respectively. According Fig. 9, the energy consumption of the translucent network design using the General algorithm is higher than when using the other two algorithms for the same BP value.

TABLE III
CAPACITY, ENERGY CONSUMPTION, INTERFACE COUNT AND NUMBER OF ALLOCATED LPS AND 3RS IN A C+L+S MBT DESIGN USING THE GENERAL, POW. OPT.
AND HYBRID ALGORITHMS AT THE BP = 1%, WITH TRAFFIC REQUEST SIZE OF 100 GB/S

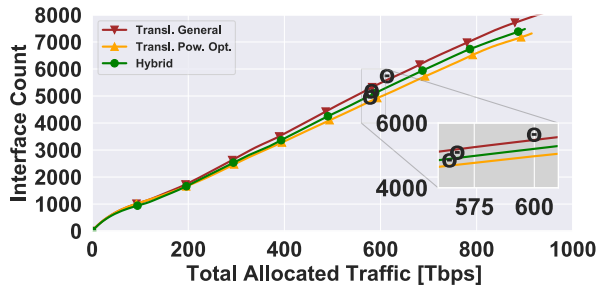| BP=10^{-2}	Capacity [Tbps]	Energy consumption [dBjpTb]	No. interfaces	No. allocated LP's	No. regenerators		
					L	C	S
General	596.52	WO Amp = 18.41 W Amp. = 19.92	5450	2725	30	117	703
Pow. Opt.	561.27	WO Amp = 18.08 W Amp. = 19.78	4658	2329	30	114	417
Hybrid	564.52	WO Amp = 18.27 W Amp. = 19.90	4896	2448	-	-	638

Fig. 10. The number of used interfaces in a translucent C+L+S MBT design using the Hybrid, General and Pow. Opt. algorithms versus total allocated traffic. The BP value of 1% is indicated in the figure by θ.

This higher energy consumption can be attributed to the fact that the main focus of this algorithm is to increase the network capacity regardless of the resulting power consumption.

Cost is obviously one of the main considerations when comparing different network upgrade solutions. Usually, in regional and long-haul networks, the interfaces are responsible for a large share of capital expenditures. Fig. 10 depicts the number of required interfaces when using the three different translucent network design algorithms versus the network total allocated traffic, along with the number of used interfaces at a BP of 1% (marked with θ). According to Fig. 10, the number of required interfaces in the translucent network design when using the Pow. Opt. algorithm is smaller than when using the General and Hybrid algorithms for the same total allocated traffic, which highlights the potential of this algorithm. As an example, for a traffic load leading to a BP=1%, the Pow. Opt. algorithm provides almost the same capacity as the Hybrid algorithm, but requires 6% (238 interfaces) fewer interfaces.

The main results of this subsection are summarized in Table III, which shows the allocated traffic, the energy consumption per Terabit, and the number of interfaces, allocated LPs, and 3R regenerators in each band. These values are obtained for a BP = 1%. From the allocated traffic viewpoint, the translucent network design using the General algorithm enables >30 Tbps additional traffic when compared to the others translucent algorithms. In terms of number of interfaces, and consequently allocated LPs, the Pow. Opt. algorithm was the one leading to the best result, requiring 4658 and 2329, respectively. Moreover, as expected, the algorithm leading to higher cost was the General one, requiring 5450 interfaces and 2725 allocated LPs to carry all traffic load. Additionally, the S-band, given its lower QoT, used the vast majority of 3R signal regenerators. Conversely, the L-band required the least amount of regenerators, in view of

its higher QoT. Particularly, the number of 3R regenerators in the L-band was kept constant (30), independently of using the General or Pow. Opt. algorithm. On the contrary, for the S-band, this value is considerably reduced to about 400 when using the Pow. Opt. algorithm instead of the General one (which required using about 700 3R regenerators). These results highlight once more the potential of the Pow. Opt. algorithm to decreases power consumption in a network by limiting the deployment of 3R regenerator at intermediate nodes. In the Hybrid network design, 638 3R regenerators are required to improve the capacity of LPs in the S-band to attain similar capacity as the one of those in the L- and C-bands. We remark that the total number of 3R regenerators required by Pow. Opt. algorithm is much smaller than the one of the Hybrid algorithm, even though similar network capacity is achieved in both cases. Consequently, in the IV-B subsection, only the transparent and translucent with General and Pow. Opt. algorithms MBT designs are compared.

B. MBT Design Comparison

In this section, the statistical network assessment results for several MBT scenarios are depicted, considering transparent and translucent network designs, with the latter using either the General or Pow. Opt. algorithms for 3R regenerators deployment.

1) Load: Fig. 11(a) shows the network allocated traffic for a BP ranging from 10^{-4} to 10^{-1}. The performance of a transparent network with C-band only transmission with ideal Shannon interfaces is also presented for benchmarking purposes (ideal C, depicted with a purple dashed-dot line with ✖ markers). This figure shows that exploiting more transmission bands increases the network capacity due to the higher number of available wavelengths. It is also noticeable that, for the same number of bands being exploited, the higher LP capacities obtained by deploying 3R regenerators reduce the BP with respect to the transparent network design. For example, the transparent network design with the C+L-band system has 40 Tbps less capacity than the C+L-band translucent case at a BP of 1% for any regenerator placement algorithm; this capacity difference increases with adding more transmission bands to the system. The difference between the transparent and translucent network designs increases from 8 Tbps in the C-band to approximately 200 Tbps in the C+L+S+U-band system. This increase is related to the higher probability of finding vacant capacity in already deployed LPs with the same source and destination when using more transmission bands. Moreover, the difference in allocated traffic between the General and Pow. Opt. translucent scenarios also become more significant for a higher
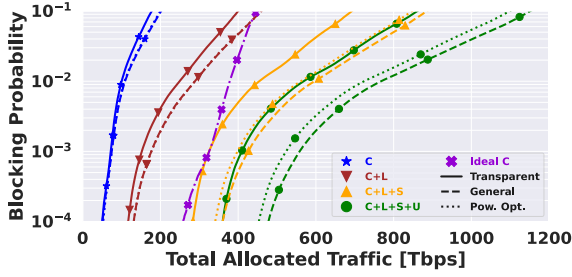
(a)
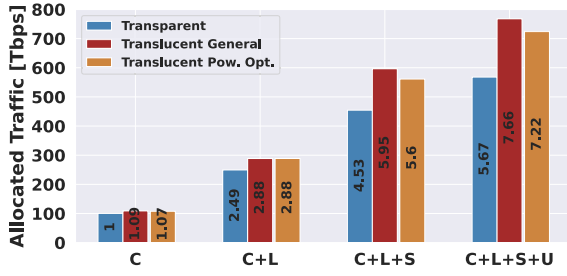
(b)

Fig. 11. Network capacity for transparent and translucent network design for the C-, C+L-, C+L+S-, and C+L+S+U-band with 100 Gb/s traffic request size a) in different BPs, and b) their capacities MFs at the BP = 1%.

(a)

(b)

Fig. 12. Network energy consumption per Terabit for transparent and translucent solution from C-, C+L-, C+L+S-, C+L+S+U-band with 100 Gb/s traffic request (a) at different BPs, and (b) their energy consumption MF at a BP = 1%. Optical amplifier power consumption is considered and the BP value of 1% is indicated in the figure by θ.

number of transmission bands. In the C- and C+L-band systems, both algorithms have almost the same behavior, whereas in the MBT C+L+S- and C+L+S+U-band scenarios their difference becomes more distinct; the translucent network designed using the General algorithm provides higher capacity. Additionally, exploiting the U-band leads to approximately the same capacity increase achieved by deploying 3R regenerators in the transparent C+L+S-band scenario. Moreover, using ideal Shannon interfaces in a transparent network design with C-band only transmission provides a better performance than using C+L-band in a transparent or translucent network. For BPs smaller than 10^{-3}, the allocated traffic of the ideal C-band scenario is comparable to the C+L+S-band system in a transparent network. This provides evidence that adopting high-end interfaces is also key to better exploiting the existing fiber infrastructure [34].

To better visualize the difference between the scenarios for a given BP, Fig. 11(b) shows the total allocated traffic for all scenarios and their MF at a BP of 1%, considering the transparent network design with the C-band only transmission as a reference. It can be observed that increasing the network capacity by exploiting more bands is more effective than deploying 3R regenerators in the C-band only scenario. Indeed, enabling the L-band in a transparent network design leads to more than twice the capacity, but performing signal regeneration only increases the network capacity by ×1.09 and ×1.07 times with the General and Pow. Opt. algorithms, respectively. In the other scenarios, a transparent network exploiting more transmission bands has almost the same or greater capacity than the translucent network. For example, the C+L+S-band translucent network has an MF value of 5.6 and 5.95, whereas the C+L+S+U-band transparent network that factor is 5.67. As the number of channels (N_{ch}) in
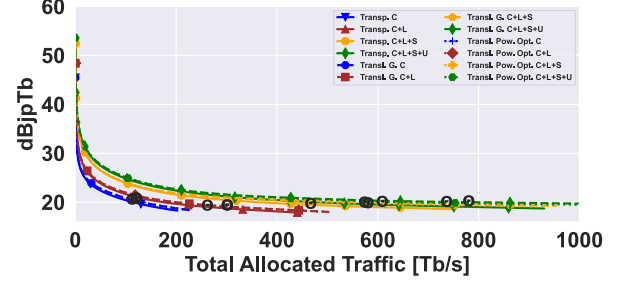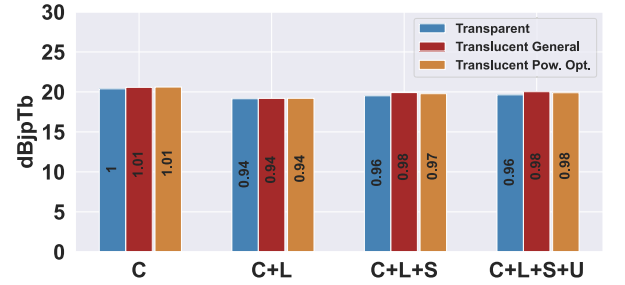
the S-band is twice as much as those in the C- and L-band, the number of available wavelengths has quadrupled and the MF has increased from ×2.5, ×2.88, and ×2.88 in the C+L-band scenario to ×4.53, ×5.95, ×5.6 times in the C+L+S-band, for the transparent, translucent General and translucent Pow. Opt. cases, respectively. Overall, these results support that exploiting more bands while keeping a transparent network design approach is an effective upgrade strategy. The translucent network design can also be used to augment capacity but is likely not the most cost-effective approach to accomplish this goal.

2) Energy: Fig. 12(a) shows the energy consumption per transmitted bit as a function of the total allocated traffic for all the scenarios, considering the interfaces' and the optical amplifiers' power consumption. The figure indicates that the consumed energy per Terabit is very high at the beginning of the network loading phase. This behavior is due to the fact that many of the LPs established have spare capacity but are already consuming the same amount of power as if they were being fully used. As new LPs are established, and some requests use the free capacity of already-deployed LPs, the energy consumption is reduced from approximately 55 dBjpTb down to around 20 dBjpTb.

Although exploiting more bands and deploying 3R regenerators increases power consumption, it also leads to higher network capacities. Fig. 12(b) shows the energy consumption per Terabit and the MF of all scenarios for a BP of 1%. This figure indicates that the energy consumption per Terabit is very similar for all scenarios. This behavior is related to the higher probability of new requests exploiting the free capacity in already deployed
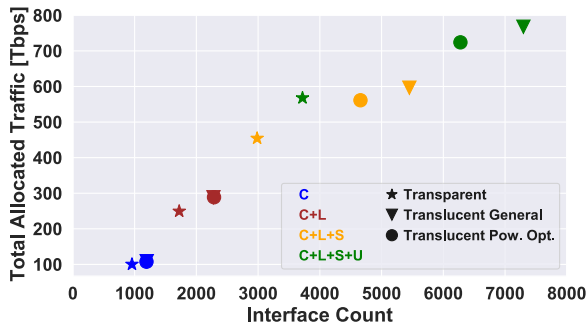
Fig. 13.   The number of used point-to-point interface numbers versus total allocated traffic with 100 Gb/s traffic request size at the BP of 1% for transparent and translucent network design from the C-band only to the C+L+S+U-band.
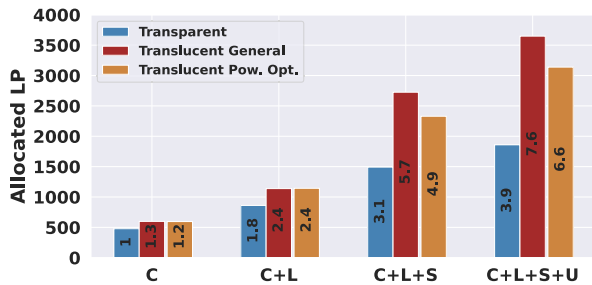

Fig. 14.   MF at the BP of 1% for the allocated LPs with 100 Gb/s traffic request size for transparent and translucent network design from the C-band only to the C+L+S+U-band.

LPs with a higher number of available wavelengths. Consequently, for a given BP, the capacity increases more than or is equal to the energy consumption for all upgrade scenarios (even with the worse QoT of additional bands). We observed similar MF values for all the scenarios as we considered a fixed BP of 1%. However, the energy consumption would change if we considered the same network capacity. For instance, at a network capacity of 200 Tbps, the consumed energy is about 19 dBjpTb in the transparent and translucent network types with the C-band. However, this value increases to 23 dBjpTb in the C+L+S+U transparent scenario due to the additional amplifiers power consumption, which leads to a change in MF value from $\times 0.96$ to $\times 1.21$ times. These results highlight the importance of using a pay-as-you-grow approach, i.e., only deploying additional bands when the links congestion increases and the target threshold BP is reached, in order to maintain high levels of energy efficiency.

3) Interface Count and Allocated LP: In this section, we show the results in terms of the number of interfaces, as a cost indicator, and the number of allocated LPs. Fig. 13 shows the interface count versus total allocated traffic at a BP of 1% for different scenarios in the transparent and translucent network designs, whereas Fig. 14 shows the total allocated LP values and MF of each scenario at a BP of 1%. The transparent network design with C-band only transmission was considered as a reference. From Fig. 13, the difference in the number of interfaces between the transparent and translucent network designs is small in the C-band scenario. However, by exploiting more bands, this difference becomes greater, and the advantages of transparent network design outweigh those of the translucent types. For

instance, a transparent network in the C+L+S+U-band scenario uses about 3719 interfaces to give a capacity of 570 Tbps; however, a translucent network design with one band less (C+L+S) needs about 5450 interfaces to reach the same capacity at the BP of 1%. Overall, by exploiting more bands progressively the allocated traffic increases in both the transparent and translucent network designs. On the contrary, the number of interfaces in the transparent network increases slightly in comparison to the translucent network type, which has a significant increase. For instance, with respect to the reference C-band only transparent network design, which demands 956 interfaces, the number of interfaces increases less than $\times 4$ times by exploiting all C-, L-, S-, and U-band and reaches 3720 when keeping the transparent network design strategy. On the contrary, this value surges to more than $\times 7.6$ times (for a total of 7298 interfaces) in the translucent network type with the General algorithm.

As expected, the number of allocated LPs have an almost identical behavior as the number of interfaces (Fig. 14). For these results, an LP with one 3R regenerator was considered to be two distinct LPs. We observed that the number of allocated LPs sharply grows in the translucent network when adding the S-band, in contrast to the transparent case. As a result, the number of allocated LPs for the transparent network design in the C+L+S+U-band scenario increased about $\times 4$, but increased by $\times 7.6$ and $\times 6.6$ in the translucent network design with the General and Pow. Opt. algorithms, respectively. Moreover, from Fig. 11(a), although the transparent network design in the C+L+S+U-band scenario has an almost equal capacity to the translucent network design in the C+L+S-band scenario, in Figs. 14 and 13 we see that the number of interfaces and allocated LPs are approximately more than $\times 2$ times fewer in the transparent design.

4) Link Congestion: Not only transparent and translucent network designs provide different capacities, but employing signal regeneration leads to differences in link congestion. Fig. 15 shows the link congestion for the transparent and translucent network designs in the network topology investigated. Fig. 15(a) and Fig. 15(b) show the link congestion in the transparent (C+L+S+U) and translucent (C+L+S) cases at a BP=1%. These two scenarios have almost equivalent capacities of ≈ 580 Tbps. In the former, four links are almost saturated, but the congestion of some links is less than 50%. For example, the *Tucson-Salt Lake City*, *Chicago-Ithaca*, *San Diego-Las Vegas*, and *Raleigh-Knoxville* links are almost completely saturated, whereas in the translucent case the congestion of these links decreased. On the other hand, the *Boulder-Chicago* and *Portland-Seattle* links experienced an increase in congestion for the translucent case. We finally remark that the link congestion distribution for the transparent (C+L+S) with ≈ 450 Tbps capacity (shown in Fig. 15(c)) is approximately the same as for the transparent (C+L+S+U) scenario (shown in Fig. 15(a)). A more detailed analysis of the link congestion shows that the average link congestion in the transparent cases (C+L+S+U and C+L+S-band transmission) is about 38%. However, signal regeneration in the translucent network design leads to an average link congestion increase of about 5%, exceeding 43% in average. Moreover, among all links between transparent network design
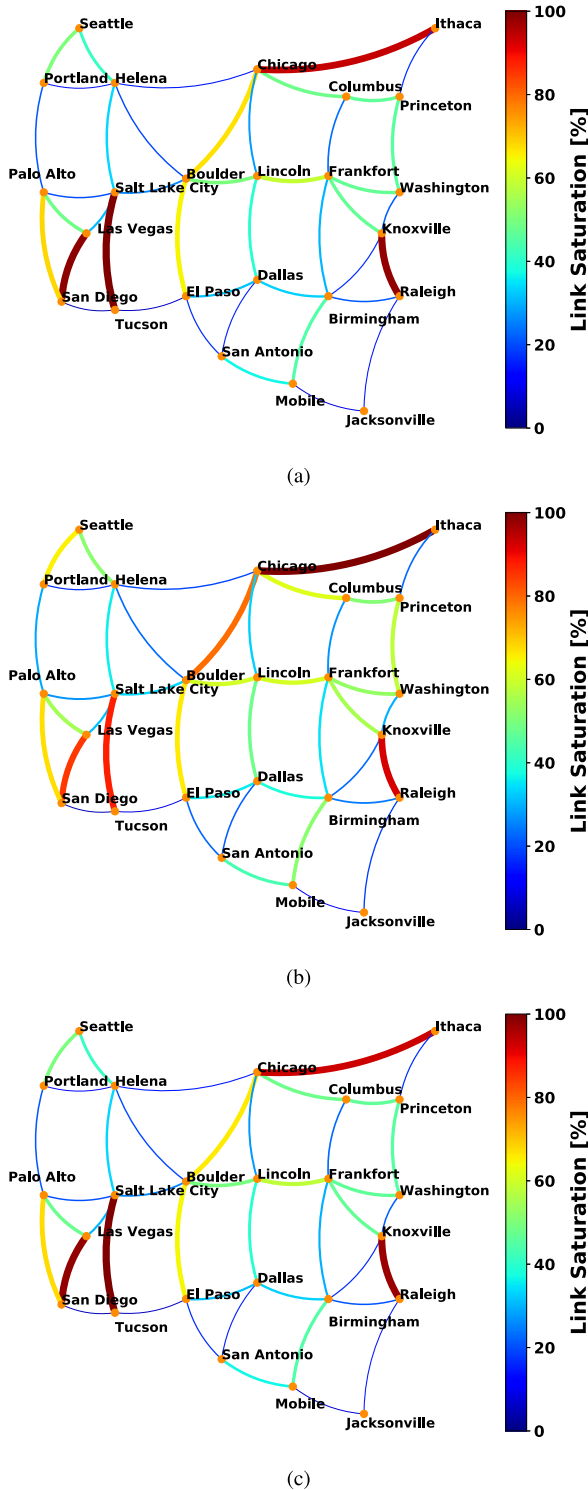
Fig. 15.   Link congestion at a BP of 1% for a) transparent (C+L+S+U), b) translucent (C+L+S), and c) transparent (C+L+S) network design.

in the CL+S+U-band and translucent network design in the C+L+S-band, the link that has changed the most due to signal generation is the *Chicago-Ithaca* and its congestion increased more than 15% because of signal regeneration in the translucent network design. On the contrary, the link of *El Paso-San Antonio* is the one that did not face any charges in its congestion.

V. CONCLUSION

In conclusion, we comprehensively analyzed the MBT transparent and translucent network designs in terms of capacity, energy consumption per Terabit, interface count, allocated LPs, and link congestion. Moreover, we have evaluated the QoT by an accurate physical layer model considering different combinations of spectral occupation within an MBT network scenario, analyzing the C-, C+L-, C+L+S-, and C+L+S+U-band scenarios. For a translucent network design, three algorithms were considered: the General, Pow. Opt., and Hybrid. Each algorithm enforces a different strategy to assign 3R regenerators to increase capacity. Results showed that focusing signal regeneration in poor-QoT bands leads to a comparable network capacity increase than using signal regeneration in all bands. Network-wide analyses indicated that exploiting an additional band in a transparent network scenario leads to the same or more capacity compared to the translucent network with the already-in-use band(s) and results in no additional energy consumption at the same BP. Moreover, we showed that, depending on the number of bands exploited, MBT translucent network design can utilize more than two times the number of interfaces compared to an MBT transparent network. It also observed that signal regeneration leads to changes in the link congestion distribution in a network. In summary, MBT transparent optical transmission is a cost-effective solution to augment the network capacity without significant increases in both cost and energy consumption.

REFERENCES

[1] "CAGR Cisco prediction 2018–2023," [Online]. Available: https://www.cisco.com/c/en/us/solutions/collateral/executive-perspectives/annual-internet-report/white-paper-c11-741490.html

[2] F. Musumeci, M. Tornatore, and A. Pattavina, "A power consumption analysis for IP-over-WDM core network architectures," *J. Opt. Commun. Netw.*, vol. 4, pp. 108–117, Feb. 2012.

[3] A. Ferrari *et al.*, "Assessment on the achievable throughput of multi-band ITU-T G. 652. D fiber transmission systems," *J. Lightw. Technol.*, vol. 38, no. 16, pp. 4279–4291, 2020.

[4] R. Sadeghi *et al.*, "Multi bands network performance assessment for different system upgrades," in *Proc. IEEE Photon. Conf.*, 2020, pp. 1–2.

[5] A. Napoli *et al.*, "Towards multiband optical systems," in *Adv. Photon. 2018 (BGPP, IPR, NP, NOMA, Sensors, Networks, SPPCom, SOF)*, Optica Publishing Group, 2018, Paper NeTu3E.1. doi: 10.1364/NETWORKS.2018.NeTu3E.1.

[6] S. Okamoto *et al.*, "WDM transmission with wavelength adaptive modulation format allocation," in *Proc. Eur. Conf. Opt. Commun.*, 2016, pp. 20–22.

[7] A. Arnould, A. Ghazisaeidi, H. Mardoyan, P. Brindel, M. Ionescu, and J. Renaudier, "High-speed and ultra-wideband devices for coherent transmission: Challenges and opportunities," in *Proc. 22nd Int. Conf. Transp. Opt. Netw.*, 2020, pp. 1–4.

[8] A. Ferrari, E. Virgillito, and V. Curri, "Band-division vs. space-division multiplexing: A network performance statistical assessment," *J. Lightw. Technol.*, vol. 38, no. 5, pp. 1041–1049, 2020.

[9] D. Semrau, E. Sillekens, R. I. Killey, and P. Bayvel, "The benefits of using the S-band in optical fiber communications and how to get there," in *Proc. IEEE Photon. Conf.*, 2020, pp. 1–2.

[10] M. Ionescu *et al.*, "74.38 tb/s transmission over 6300 km single mode fibre enabled by C+ L amplification and geometrically shaped PDM-64QAM," *J. Lightw. Technol.*, vol. 38, no. 2, pp. 531–537, 2020.

[11] M. Cantono, R. Schmogrow, M. Newland, V. Vusirikala, and T. Hofmeister, "Opportunities and challenges of C+ L transmission systems," *J. Lightw. Technol.*, vol. 38, no. 5, pp. 1050–1060, 2019.

[12] A. Ferrari, D. Pilori, E. Virgillito, and V. Curri, "Power control strategies in C+ L optical line systems," in *Proc. Opt. Fiber Commun. Conf. Exhibit.*, 2019, pp. 10–12.

[13] I. Roberts, J. M. Kahn, J. Harley, and D. W. Boertjes, "Channel power optimization of WDM systems following Gaussian noise nonlinearity model in presence of stimulated Raman scattering," *J. Lightw. Technol.*, vol. 35, pp. 5237–5249, 2017.

[14] D. Moniz, V. Lopez, and J. Pedro, "Design strategies exploiting C+L-band in networks with geographically-depedent fiber upgrade expenditures," in *Proc. Opt. Fiber Commun. Conf. Exhibit.*, 2020, pp. 1–3.

[15] V. Lopez et al., "Optimized design and challenges for C&L band optical line systems," *J. Lightw. Technol.*, vol. 38, no. 5, pp. 1080–1091, 2020.

[16] G. Shen and R. S. Tucker, "Translucent optical networks: The way forward [*topics in optical communications*]," *IEEE Commun. Mag.*, vol. 45, no. 2, pp. 48–54, Feb. 2007.

[17] E. Karasan and M. Arisoylu, "Design of translucent optical networks: Partitioning and restoration," *Photon. Netw. Commun.*, vol. 8, no. 2, pp. 209–221, 2004.

[18] G. Shen, W. Grover, T. Cheng, and S. Bose, "Sparse placement of electronic switching nodes for low blocking in translucent optical networks," *J. Opt. Netw.*, vol. 1, no. 12, pp. 424–441, 2002.

[19] G. Shen and W. Grover, "Segment-based approaches to survivable translucent network design under various ultra-long-haul system reach capabilities," *J. Opt. Netw.*, vol. 3, no. 1, pp. 1–24, 2004.

[20] X. Yang and B. Ramamurthy, "Sparse regeneration in translucent wavelength-routed optical networks: Architecture, network design and wavelength routing," *Photon. Netw. Commun.*, vol. 10, no. 1, pp. 39–53, 2005.

[21] M. Klinkowski, "On the effect of regenerator placement on spectrum usage in translucent elastic optical networks," in *Proc. 14th Int. Conf. Transp. Opt. Netw.*, 2012, pp. 1–6.

[22] R. Sadeghi et al., "Performance comparison of translucent C-band and transparent C + L-band network," in *Proc. Opt. Fiber Commun. Conf. Exhib.*, 2021, pp. 1–3.

[23] J. M. Simmons, *Optical Network Design and Planning*. Berlin, Germany: Springer, 2014.

[24] J. Pedro, "Predeployment of regenerators for fast service provisioning in DWDM transport networks," *J. Opt. Commun. Netw.*, vol. 7, pp. A 190–A 199, Feb. 2015.

[25] D. A. R. Chaves, E. F. da Silva, C. J. A. Bastos-Filho, H. A. Pereira, and R. C. Almeida, "Heuristic algorithms for regenerator assignment in dynamic translucent elastic optical networks," in *Proc. 17th Int. Conf. Transp. Opt. Netw.*, 2015, pp. 1–4.

[26] S. Rumley and C. Gaumier, "Cost aware design of translucent WDM transport networks," in *Proc. 11th Int. Conf. Transp. Opt. Netw.*, 2009, pp. 1–4.

[27] Z. Pan, B. Chatelain, D. V. Plant, F. Gagnon, C. Tremblay, and E. Bernier, "Tabu search optimization in translucent network regenerator allocation," in *Proc. IEEE 5th Int. Conf. Broadband Commun., Netw. Syst.*, 2008, pp. 627–631.

[28] M. Kanj, E. L. Rouzic, J. Meuric, and B. Cousin, "Optical power control in translucent flexible optical networks with GMPLS control plane," *J. Opt. Commun. Netw.*, vol. 10, pp. 760–772, Sep. 2018.

[29] B. Ramamurthy, H. Feng, D. Datta, J. P. Heritage, and B. Mukherjee, "Transparent vs. opaque vs. translucent wavelength-routed optical networks," in *Proc. IEEE OFC/IOOC. Tech. Digest. Opt. Fiber Commun. Conf., Int. Conf. Integr. Opt. Opt. Fiber Commun.*, vol. 1, 1999, pp. 59–61.

[30] F. Frey, R. Elschner, and J. K. Fischer, "Estimation of trends for coherent DSP ASIC power dissipation for different bitrates and transmission reaches," in *Proc. Photon. Netw., 18. ITG-Symp.*, pp. 1–8, 2017.

[31] M. Kuschnerov, T. Bex, and P. Kainzmaier, "Energy efficient digital signal processing," in *Proc. Opt. Fiber Commun. Conf.*, 2014, Paper Th3E.

[32] "OIF 400ZR IA," [Online]. Available: https://www.oiforum.com/wp-content/uploads/OIF-400ZR-01.0_reduced2.pdf

[33] "Open ZR MSA technical specification," [Online]. Available: https://openzrplus.org/site/assets/files/1075/openzrplus_1p0.pdf

[34] J. Pedro, N. Costa, and S. Sanders, "Scaling regional optical transport networks with pluggable and integrated high-capacity line interfaces," in *Proc. Opt. Fiber Commun. Conf.*, OSA, 2021, Paper M3E.1.

[35] V. Curri, M. Cantono, and R. Gaudino, "Elastic all-optical networks: A new paradigm enabled by the physical layer. how to optimize network performances?," *J. Lightw. Technol.*, vol. 35, pp. 1211–1221, Mar. 2017.

[36] E. Virgillito, R. Sadeghi, A. Ferrari, A. Napoli, B. Correia, and V. Curri, "Network performance assessment with uniform and non-uniform nodes distribution in C+ L upgrades vs. fiber doubling SDM solutions," in *Proc. Int. Conf. Opt. Netw. Des. Modelling*, 2020, pp. 1–6.

[37] E. Virgillito, R. Sadeghi, A. Ferrari, G. Borraccini, A. Napoli, and V. Curri, "Network performance assessment of C + L upgrades vs. fiber doubling SDM solutions," in *Proc. Opt. Fiber Commun. Conf.*, OSA, 2020, Paper M2G.4.

[38] M. Cantono et al., "On the interplay of nonlinear interference generation with stimulated Raman scattering for QoT estimation," *J. Lightw. Technol.*, vol. 36, no. 15, pp. 3131–3141, 2018.

[39] V. Kamalov et al., "The subsea fiber as a Shannon channel," in *Proc. SubOpt.*, 2019.

[40] V. Curri, "Software-defined WDM optical transport in disaggregated open optical networks," in *Proc. Int. Conf. Transp. Opt. Netw.*, 2020, pp. 1–4.

[41] A. Ferrari et al., "GNPy: An open source application for physical layer aware open optical networks," *IEEE/OSA J. Opt. Commun. Netw.*, vol. 12, no. 6, pp. C31–C40, Jun. 2020.

[42] B. Correia et al., "Power control strategies and network performance assessment for C + L+S multiband optical transport," *J. Opt. Commun. Netw.*, vol. 13, pp. 147–157, Jul. 2021.

[43] M. Filer, J. Gaudette, Y. Yin, D. Billor, Z. Bakhtiari, and J. L. Cox, "Low-margin optical networking at cloud scale," *J. Opt. Commun. Netw.*, vol. 11, no. 10, pp. C94–C108, 2019.

[44] Y. Ando, "Statistical analysis of insertion-loss improvement for optical connectors using the orientation method for fiber-core offset," *IEEE Photon. Technol. Lett.*, vol. 3, no. 10, pp. 939–941, Oct. 1991.

[45] V. Curri et al., "Design strategies and merit of system parameters for uniform uncompensated links supporting Nyquist-WDM transmission," *J. Lightw. Technol.*, vol. 33, no. 18, pp. 3921–3932, 2015.

[46] B. Correia, R. Sadeghi, E. Virgillito, A. Napoli, and V. Curri, "Optical power control strategies for optimized C+L+S-bands network performance," in *Proc. Opt. Fiber Commun. Conf. Exhib.*, 2021, pp. 1–3.

[47] R. Sadeghi et al., "Optimized translucent S-band transmission in multi-band optical networks," in *Proc. Eur. Conf. Opt. Commun.*, 2021, pp. 1–4.

[48] J. Pedro and S. Pato, "Capacity increase and hardware savings in DWDM networks exploiting next-generation optical line interfaces," in *Proc. 20th Int. Conf. Transparent Opt. Netw.*, 2018, pp. 1–6.

[49] "C-band optical amplifier (EDFA)," [Online]. Available: https://www.fiberlabs.com/1u_amp/1500nm-1u-amp/

[50] "L-band optical amplifier (EDFA)," [Online]. Available: https://www.fiberlabs.com/1u_amp/1600nm-1u-amp/

[51] "S-band optical amplifier (TDFA)," [Online]. Available: https://www.fiberlabs.com/bt_amp_index/s-band-bt-amp/